Received: 5 August 2022 | Revised: 17 October 2022 | Accepted: 5 November 2022

DOI: 10.1002/pro.4509

FULL-LENGTH PAPER

THE PROTEIN SOCIETY WILEY

Biophysical characterization of full-length TAR DNA-binding protein (TDP-43) phase separation

Tommaso Staderini | **Alessandra Bigi** | **Daniele Mongiello** | **Cristina Cecchi** | **Fabrizio Chiti**

Department of Experimental and Clinical Biomedical Sciences "Mario Serio", University of Florence, Florence, Italy

Correspondence
Fabrizio Chiti, Department of Experimental and Clinical Biomedical Sciences "Mario Serio," University of Florence, Florence 50134, Italy.
Email: fabrizio.chiti@unifi.it

Funding information
Fondazione Cassa di Risparmio di Firenze, Grant/Award Number: Projects TROTHERALS and TDP43SLA; Fondazione Italiana di Ricerca per la Sclerosi Laterale Amiotrofica, Grant/Award Number: Project TDP-43-Struct; Ministero dell'Università e della Ricerca, Grant/Award Number: Project PRIN n. 2020PBS5MJ; Università degli Studi di Firenze, Grant/Award Number: Fondi di ateneo

Review Editor: John Kuriyan

Abstract

Amyotrophic lateral sclerosis and frontotemporal lobar degeneration with ubiquitin-positive inclusions are associated with deposition of cytosolic inclusion bodies of TAR DNA-binding protein 43 (TDP-43) in brain and motor neurons. We induced phase separation of purified full-length TDP-43 devoid of large tags using a solution-jump method, and monitored it with an array of biophysical techniques. The tetramethylrhodamine-5-maleimide- or Alexa488-labeled protein formed rapidly (<1 min) apparently round, homogeneous and 0.5–1.0 μm wide assemblies, when imaged using confocal fluorescence, bright-field, and stimulated emission depletion microscopy. The assemblies, however, had limited internal diffusion, as assessed with fluorescence recovery after photobleaching, and did not coalesce, but rather clustered into irregular bunches, unlike those formed by the C-terminal domain. They were enriched with α-helical structure, with minor contributions of β-sheet/random structure, had a red-shifted tryptophan fluorescence and did not bind thioflavin T. By monitoring with turbidimetry both the formation of the spherical species and their further clustering under different experimental conditions, we carried out a multiparametric analysis of the two phenomena. In particular, both processes were found to be promoted by high protein concentrations, salts, crowding agents, weakly by reducing agents, as the pH approached a value of 6.0 from either side (corresponding to the TDP-43 isoionic point), and as the temperature approached a value of 31°C from either side. Important differences were found with respect to the TDP-43 C-terminal domain. Our multiparametric results also provide explanations to some

Abbreviations: ALS, amyotrophic lateral sclerosis; CD, circular dichroism; C_{sat}, protein concentration above saturation; CTD, C-terminal domain; D_h, hydrodynamic diameter; DLS, dynamic light scattering; FRAP, fluorescence recovery after photobleaching; FTLD-TDP, frontotemporal lobal degeneration with TDP-43 positive inclusions; FTLD-U, frontotemporal lobal degeneration with ubiquitin positive inclusions; GOF, gain-of-function; GSH, reduced glutathione; GSSG, glutathione disulfide; HEPES, 4-(2-hydroxyethyl)-1-piperazineethanesulfonic acid; IEX, ion exchange chromatography; IPTG, isopropyl β-D-1-thiogalatoside; LDAO, dodecyldimethylaminoxid; LLPS, liquid–liquid phase separation; LOF, loss-of-function; MBP, maltose binding protein; MWCO, molecular weight cut-off; NES, nuclear export signal; Ni-NTA, HisPur Ni-nitrilotriacetic acid; NLS, nuclear localization signal; NTD, N-terminal domain; OG, octyl-β-D-glucopyranoside; PEG 3350, polyethylene glycol 3350; PEG 8000, polyethylene glycol 8000; QFF, Q-Sepharose Fast Flow; ROIs, regions of interest; RRMs, RNA recognition motifs; SEC, size-exclusion chromatography; SGs, stress granules; STED, stimulated emission depletion; SUMO, small ubiquitin-like modifier; TCEP, tris(2-carboxyethyl)phosphine; TDP-43, TAR DNA-binding protein 43; TEM, transmission electron microscopy; ThT, thioflavin; TMR, tetramethylrhodamine-5-maleimide; YFP, yellow fluorescent protein.

of the solubility data obtained on full-length TDP-43 that were difficult to explain following the multiparametric analysis acquired on the C-terminal domain.

KEYWORDS

ALS, FTLD, liquid–liquid phase separation, motor neuron diseases, recombinant TDP-43, self-assembly

1 | INTRODUCTION

Amyotrophic lateral sclerosis (ALS) and frontotemporal lobar degeneration with ubiquitin positive inclusions (FTLD-U or FTLD-TDP) are associated with a common histopathology, consisting in the formation of cytosolic inclusion bodies (IBs) of the nuclear TAR DNA-binding protein 43 (TDP-43) in neurons of the central nervous system.[1–4] In the cytosol, the protein loses its solubility and forms well defined skein-like or round inclusions, where TDP-43 is hyperphosphorylated, polyubiquitinated, and in part proteolyzed to form C-terminal fragments.[1–3,5,6] It is increasingly recognized that ALS and FTLD-TDP consist in a combination of loss-of-function (LOF), originating from the depletion of TDP-43 from the nucleus with a consequently loss of its biological function, and a gain-of-function (GOF), resulting from the formation of TDP-43 assemblies that act as saboteurs in the cytosol.[7–10] TDP-43 inclusions are also frequently found in the brain of Alzheimer's disease,[11] Parkinson's disease,[12] Huntington's disease,[13] and other neurodegenerative conditions,[14] emphasizing its high propensity to aggregate in a wide spectrum of neurologically compromised situations.

TDP-43 is a 414-residue protein consisting of an N-terminal domain (NTD, residues 1–76), two RNA recognition motifs (RRM1, residues 106–176; RRM2, residues 191–259), and a C-terminal domain (CTD, residues 274–414). While the first three domains are folded and their structures have been determined using solution NMR spectroscopy or X-ray crystallography,[15] the CTD consists of a prion-like glutamine/asparagine-rich (Q/N) region (residues 345–366), a glycine-rich region (residues 366–414) and is intrinsically disordered with an amphipathic helix spanning approximately residues 320–340.[16,17] TDP-43 also contains a nuclear localization signal (NLS, residues 82–98) and a nuclear export signal (NES, residues 239–250), and is known to have a nuclear localization but also to shuttle between the nucleus and the cytosol.[18] TDP-43 was first proposed to be natively dimeric or at least to exist in a monomer–dimer equilibrium under normal physiological conditions, with dimerization occurring through interactions of the NTDs.[19–22] Later on, isolated NTDs, and consequently full-length TDP-43 molecules, were found to form a head-to-tail interaction that could propagate the oligomeric structure well beyond the dimer.[23,24]

Under conventional immunohistochemistry, the TDP-43 inclusions appear either skein-like or compact and rounded.[1,2,25–27] Round inclusions range from 1 to 25 μm in diameter, whereas skein-like inclusions are about 0.5–1.0 μm in diameter and up to 15 μm in length.[4,25,26,28] In both cases, however, it is likely that smaller species are present and escape detection due to microscopical resolution limitations. Using transmission electron microscopy (TEM), histopathologists have reported repeatedly that 10–20 nm wide filaments containing TDP-43 are present within the inclusions,[11,29–32] in the absence of Congo red or thioflavin (ThT) S binding.[33–36] A recent study by cryo-electron microscopy has revealed the molecular structure of the protease-resistant core of the filaments extracted from the cortex of two cases with a history of ALS associated with FTLD-U.[32] In this structure, residues 282–360 from contiguous TDP-43 CTDs are stacked in a parallel, in-register mode, forming a 4.8 Å repeating unit, each time rotating by 1.4° angles to form a right-handed double-spiral fold.[32] Each 282–360 segment forms 10 very short β-strands alternated by long stretches of turns, preventing the very narrow β-sheets from stacking perpendicular to the filament axis and from forming the cross-β structure typical of amyloid fibrils observed in other diseases. The smooth and largely hydrophilic surface of the filament also appears to prevent the binding of amyloid-diagnostic dyes, such as ThT/S, which requires deep and nonpolar grooves.[32]

The conversion of soluble dimeric/oligomeric TDP-43 into solid-phase filaments that compose the round or skein-like inclusions is an unclear process. One of the complexities is the supposed tendency of TDP-43 to undergo liquid–liquid phase separation (LLPS) which forms droplets in which TDP-43 and other proteins may adopt a liquid phase separated from the bulk cytosolic solution. TDP-43 containing droplets have been identified in several nuclear and cytoplasmic membraneless organelles, such as stress granules (SGs),[37–39] cytosolic droplets independent of SGs,[40] paraspeckles,[41,42] Cajal bodies,[43]

Gemini bodies,[43] PML bodies,[43] stress-induced nuclear bodies,[44] and so forth. A liquid-to-solid transition has been found to occur within SGs,[38,40] although an SG independent formation of solid inclusions has also been observed.[38,45,46]

Much of the work on pure TDP-43 LLPS in vitro has been carried out using the isolated CTD, which is unstructured, prion-like, hosts the majority of TDP-43 mutations associated with familial ALS and is, therefore, often assumed to drive and influence self-assembly of the full-length protein. The isolated TDP-43 CTD has been found to form in vitro *bona fide* liquid droplets that have a round morphology, ability to coalesce and the dynamic behavior typical of liquids, as assessed with fluorescence recovery after photobleaching (FRAP).[16,47] A multiparametric analysis of CTD LLPS has been carried out, revealing that it is a process thermodynamically favored at high protein concentration, neutral pH (as opposed to weakly acidic pH), high salt concentrations, low temperature, presence of crowding agents.[17,47] Droplets have also been observed in vitro from pure full-length TDP-43,[48] but other reports described a difficulty of the condensates to coalesce or display rapid internal diffusion.[24,36,49,50] Moreover, all these studies have been carried out with TDP-43 fused to large solubilizing proteins, including the small ubiquitin-like modifier (SUMO), the maltose binding protein (MBP), the yellow fluorescent protein (YFP), or after their partial removal with proteolysis with no further purification, creating conditions that may alter the behavior of TDP-43 relative to the isolated tag-free protein. In addition, the dependence of phase separation on parameters of physiological relevance has not been studied in any detail for the full-length protein, or at least not as extensively as for the CTD. Finally, it is not clear if TDP-43 LLPS is an obligatory requirement for solid inclusion and filament formation or an independent occurrence.

Here, we study the phase separation behavior of purified full-length TDP-43 devoid of large tags, using an array of biophysical techniques to study the morphology of the assemblies, their state of matter, the structure of TDP-43 molecules adopted within them and to determine the multiparametric dependence of self-assembly previously attempted only for the CTD. We will not assume that phase separation is necessarily a liquid–liquid type of phase separation: with the term "phase separation," we intend the process in which the protein passes from solution into self-assemblies, regardless of their solid or liquid state. Indeed, phase separation is a generic term that includes both liquid–liquid and liquid–solid phase separations.[51] We will show that the protein forms assemblies of the order of 0.5–1.0 μm of diameter, with limited internal diffusion and tendency to assemble in chain-like arrangements without coalescence, showing a behavior distinct from the pure liquid state of TDP-43 CTD. We also find important differences between how the various parameters affect formation of these species for full-length TDP-43 and droplets for the isolated CTD.

2 | RESULTS

2.1 | Recombinant TDP-43 is pure and has proper dimeric fold

Human full-length TDP-43 was recombinantly expressed and purified with a 6x His-tag fused to the N-terminus (see Section 5 for details) and will be referred to as TDP-43 throughout the text. It was purified from bacterial IBs through refolding conditions, using a slightly modified previously published protocol,[52] as described in Section 5 in detail. Final conditions of the purified protein were 50 mM 4-(2-hydroxyethyl)-1-piperazineethanesulfonic acid (HEPES), pH 8.0, 0.1% (wt/vol) polyethylene glycol 3350 (PEG 3350), 2 mM dodecyldimethylaminoxid (LDAO), 0.25% (wt/vol) octyl-β-D-glucopyranoside (OG), 1 M NaCl. Prior to analysis, we ensured that the protein sample had a high purity, was properly folded and was not aggregated. SDS-PAGE revealed a major band corresponding to a molecular weight of ~47 kDa, in agreement with the expected value of 47.292 kDa (Figure 1a). TDP-43 fragments probably generated by proteases are also present, but these account for less than 5% of the entire protein sample (Figure 1a). Dynamic light scattering (DLS) showed the presence of a single peak with an apparent hydrodynamic diameter (D_h) of 127 ± 3 Å (Figure 1b), in agreement with the previously found value of 130 ± 3 Å and attributed to a dimeric folded form of the protein.[52] Indeed, the expected D_h values for a TDP-43 construct of this size (436 residues) and containing the first three and last domains in folded and unfolded states, respectively, are 92.3, 123.1, and 153.9 Å, for monomeric, dimeric, and higher order oligomeric forms, respectively, as determined using the previously described approach.[52] Unfolded TDP-43 was found to have a D_h value of about 190 Å,[52] indicating that the protein is not unfolded in our sample. Large aggregates are not detectable with DLS, indicating that they are also absent. The intrinsic fluorescence emission spectrum of the sample was also similar to that previously found,[52] with a wavelength of maximum emission at about 320–325 nm and three overlapping peaks in the 320–350 nm range, attributable to Trp residues with different degrees of burial (Figure 1c). Hence, the data confirm the proper folding and dimeric state of TDP-43, being consistent with those proposed previously.[52]

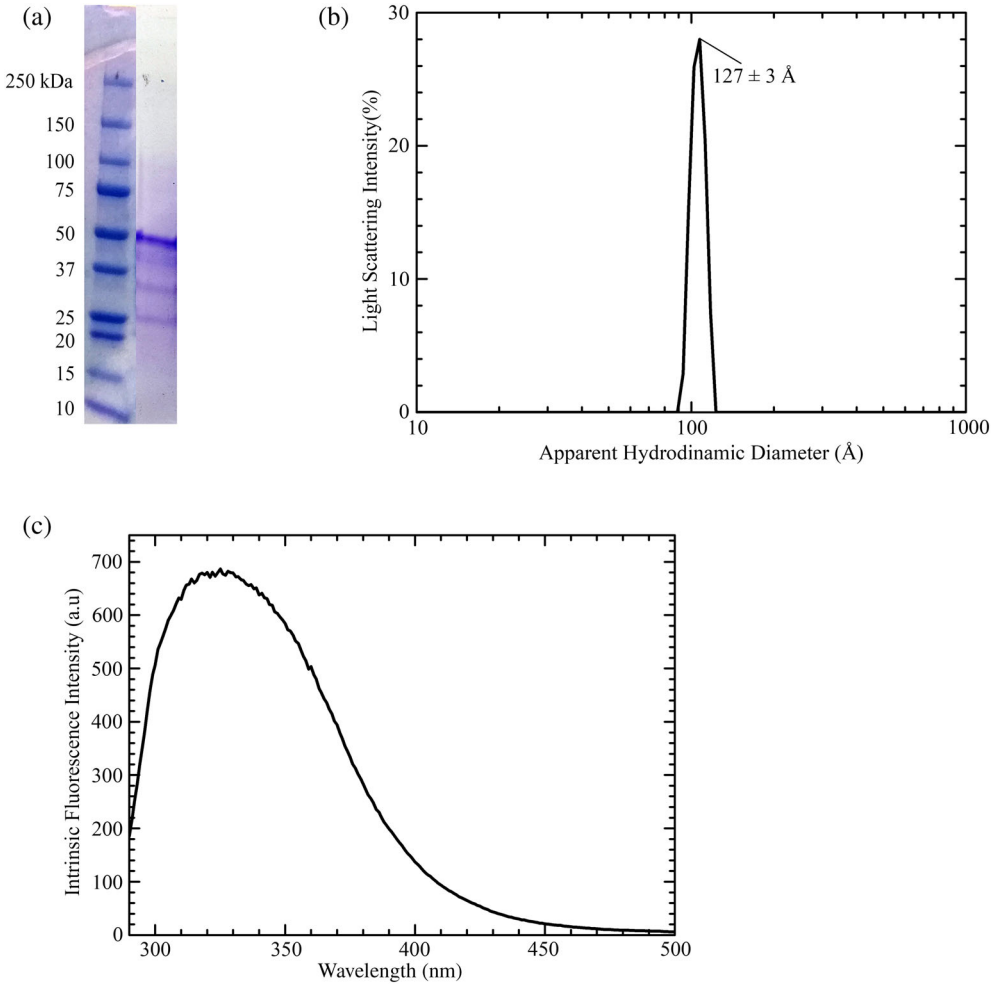

FIGURE 1 Preliminary characterization of purified TDP-43. (a) SDS-PAGE of purified TDP-43. (b) Particle size distribution of TDP-43 determined with DLS. (c) Intrinsic fluorescence spectrum of TDP-43 (excitation of 280 nm). a.u, arbitrary units. Analysis was carried out in QFF Buffer B (see Section 5) at 25°C

2.2 | TDP-43 assemblies do not have liquid-like characteristics

In order to assess the propensity of TDP-43 to phase separate in vitro, the protein was diluted from the initial solution described above in which it was soluble, at a protein concentration of 35 μM, into another solution in which it was not soluble, at a final protein concentration of 5 μM, specifically in 20 mM acetate buffer, pH 5.0, 5% (wt/vol) PEG 8000, 2 mM tris(2-carboxyethyl)phosphine (TCEP), 25°C (to reach a final pH 6.0 after dilution), containing either 0 mM or 150 mM NaCl, as described in Section 5. With the term "phase separation," we intend the process in which the protein passes from solution into self-assemblies, regardless of their solid or liquid state. Indeed, phase separation is a generic term that includes both liquid–liquid and liquid–solid phase separations.[51]

To examine the size and morphology of the TDP-43 self-assemblies, we performed live imaging of TDP-43 labeled with the tetramethylrhodamine-5-maleimide (TMR) fluorescent probe (TDP-43-TMR) by confocal fluorescence and bright-field microscopy, at different time points after phase-separation induction, at the two NaCl concentrations considered here (Figures 2a and S1a). At 150 mM NaCl and 0 min, confocal images revealed the presence of typically ~0.5–1.0 μm round-shaped assemblies (Figure 2a), although smaller species may also be present and escape detection.[53,54] Larger round species with diameters of 1–2 μm were also occasionally imaged, albeit rarely.

By performing live 2D and 3D imaging of individual round TDP-43-TMR assemblies by stimulated emission depletion (STED) confocal fluorescence microscopy, and by recording superimposed and median level 2D images without and with deconvolution to gain morphological resolution at 0.01 μm, the assemblies appeared homogenous in fluorescence and did not show any appearance of filamentous or other type of morphology, which would be evident at this resolution power (Figure S2). The images also revealed that the condensate had a good degree of roundness, which did not appear, however, as high as that expected for liquid droplets, due to the presence of stretched and squashed regions on the borders (Figure S2).

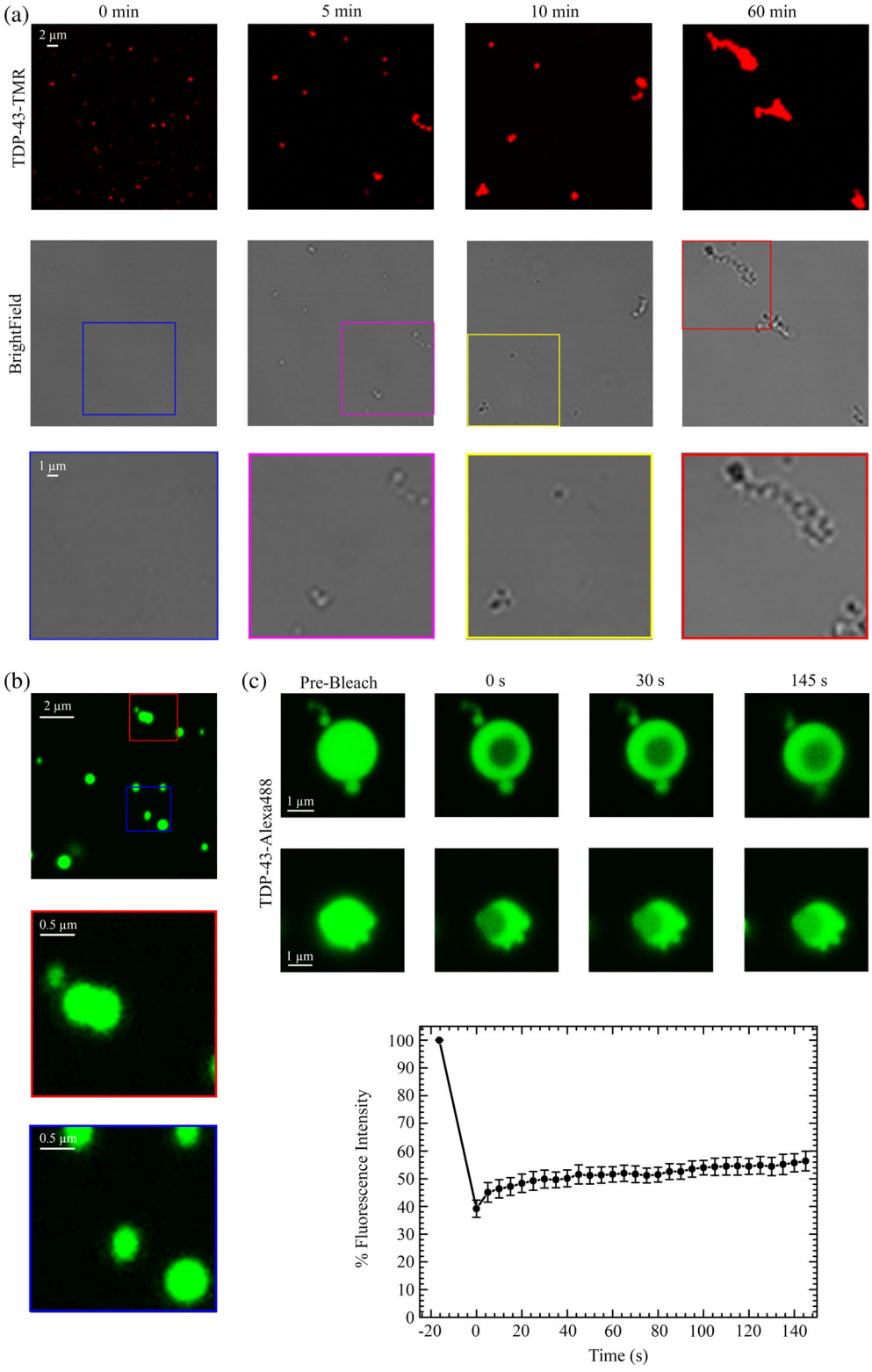

FIGURE 2 Confocal fluorescence and bright-field microscopy images and FRAP of TDP-43 assemblies. (a) Representative confocal fluorescence and bright-field images of TDP-43-TMR during phase separation. Self-assembly was induced by a solution-jump method, diluting the protein from its initial solution, where it was soluble and native, into a solution in which it was insoluble (20 mM acetate buffer, pH 5.0, 150 mM NaCl, 5% (wt/vol) PEG 8000, 2 mM TCEP, 25°C). The experiment occurred at final pH of 6.0, 25°C and the TDP-43 concentration was 5 μM. In the third line, higher magnifications of bright-field images are shown in the colored boxed areas. (b) Representative confocal fluorescence images of 5 μM TDP-43-Alexa488 treated as described in Panel (a) and recorded at 0 min. Higher magnifications of the images are shown in the colored boxed areas. (c) Representative images from FRAP experiments on two distinct assemblies (0 min). An averaged time course graph of FRAP carried out on five distinct assemblies is shown. Fluorescence was normalized to pre-bleach fluorescence values (taken as 100%). Error bars: *SEM*

At 5 min, a few assemblies appeared to form irregular, non-rounded clusters, indicating their tendency to assemble further without any sign of coalescence (Figure 2a). At this time, the protein sample was heterogeneous, given the co-existence of ~0.5–1.0 μm round condensates and larger clusters. At 10 min, the irregular clusters appeared bigger, indicating further assembly, still in the absence of coalescence (Figure 2a). After 60 min, the assemblies were very large, irregular in shape and the initial 0.5–1.0 μm round species were scarce (Figure 2a). At 0 mM NaCl, a similar scenario was observed, but TDP-43 tended to phase separate less effectively, forming

fewer and smaller assemblies than at higher ionic strength, and the conversion into larger species also appeared to be delayed to some extent (Figure S1a).

To investigate the state of matter of the round assemblies, we set up FRAP experiments on TDP-43 labeled with Alexa Fluor 488 (TDP-43-Alexa488). In this experiment, we used AlexaFluor 488 because it is more suitable for photobleaching than TMR, which is, by contrast, very hard to bleach. Figure 2b shows the assemblies before FRAP imaged at 0 min, confirming that they had a size of typically ~0.5–1.0 μm (only few species had a diameter >1 μm), round shape and inability to coalesce when interacting, which is particularly evident in magnification boxes. Representative big assemblies were selected for FRAP experiments (Figure 2c). The quantitative analysis revealed a first phase of low fluorescence recovery from a value of about 30% (after photobleaching) to a value of about 50% (after recovery), followed by a slow low amplitude recovery up to a value of about 55% after 140 s, thus indicating a low mobility of TDP-43 molecules inside the assemblies and absence of a purely liquid-like state. Very similar results were obtained when FRAP experiments were conducted at 0 mM NaCl (Figure S1b,c). In this case, we were able to trap a higher number of round species interacting together, again showing no tendency to coalesce.

2.3 | TDP-43 phase separation is monitorable with turbidimetry and is not accompanied with amyloid-like structure

We triggered again TDP-43 self-assembly using the same solution-jump procedure described in the previous section and monitored the process with turbidimetry, intrinsic fluorescence, ThT assay and far-UV circular dichroism (CD). At both NaCl concentrations, the turbidity time course (OD_{600}) revealed a rapid increase of turbidity immediately after dilution (0 min), with a maximum value after 5–10 min of incubation and then gradually decreased down to a value close to zero (Figure 3a and S3a). By comparing the microscopic and turbidimetry data, it is clear that the initial increase of turbidity is associated with the formation of the small spherical assemblies and their smallest clusters, whereas the second slower decrease is associated with formation of the large clusters that "clear" the solution from the small species causing turbidity.

Both far-UV CD spectra at 0 and 150 mM NaCl recorded at 0 min after the solution jump are enriched with α-helical structure, as indicated by negative minima at ~222 and ~208 nm (Figures 3b and S3b). This indicates that the protein molecules adopt α-helical structure, possibly mixed with a lower content of β-sheet and disordered structure, within the initial aggregates, as often observed in phenomena of protein self-assembly. As the incubation time elapses, a blue shift of the second peak from ~208 to ~204 nm and, concomitantly, a reduction of the signal at 222 nm, reveal the tendency of the protein to lose some of its initial α-helical/β-sheet structure and undergo incomplete unfolding (Figures 3b and S3b). Interestingly, the CD spectra did not show any evident peak around 215–220 nm or 225 nm, typical of β-sheet structure in small species and β-sheet structure within large protein aggregates, respectively. This suggests the lack of species having a predominant β-sheet content, forming during the process, and rules out the presence of amyloid-like structure (Figures 3b and S3b).

Intrinsic Trp fluorescence spectra showed a red shift of the major intrinsic fluorescence peak of the native non-phase separated protein, from the wavelength value at about 320–325 nm to around 335–340 nm, which suggests that the protein is not completely unfolded within the aggregates and that buried Trp residues become more exposed to the bulk due to structural adjustment (Figures 3c and S3c).

ThT fluorescence spectra of TDP-43 showed a heavy wavelength-dependent and ThT-independent light scattering effect that increased the apparent fluorescence emission due to the growing presence of protein assemblies over time (Figures 3d and S3d). However, TDP-43 samples showed a weak increase of fluorescence intensity at 485 nm over the light-scattering baseline, similarly to that observed for the native protein over the ThT spectrum in the absence of protein taken as a blank (Figures 3d and S3d). This suggests that TDP-43 did not form any amyloid-like structure in our experimental setting, because the small ThT fluorescence increase observed here is in sharp contrast with the over fivefold fluorescence increase expected for amyloid.[55,56]

2.4 | Multi-parametric turbidimetry shows how phase separation can be tuned

In order to investigate the multiparametric dependence of TDP-43 self-assembly, we carried out kinetic assays by monitoring the absorbance at 600 nm (turbidimetry) of TDP-43 as a function of time and changing the various parameters one by one while keeping the remaining ones constant. To this purpose, we selected the following solutions as our standard condition: 5 μM TDP-43 in 20 mM acetate buffer, pH 5.0, 5% (wt/vol) PEG 8000, 2 mM TCEP, 25°C (to reach a final pH 6.0 after dilution), containing either 0, 50, or 150 mM NaCl.

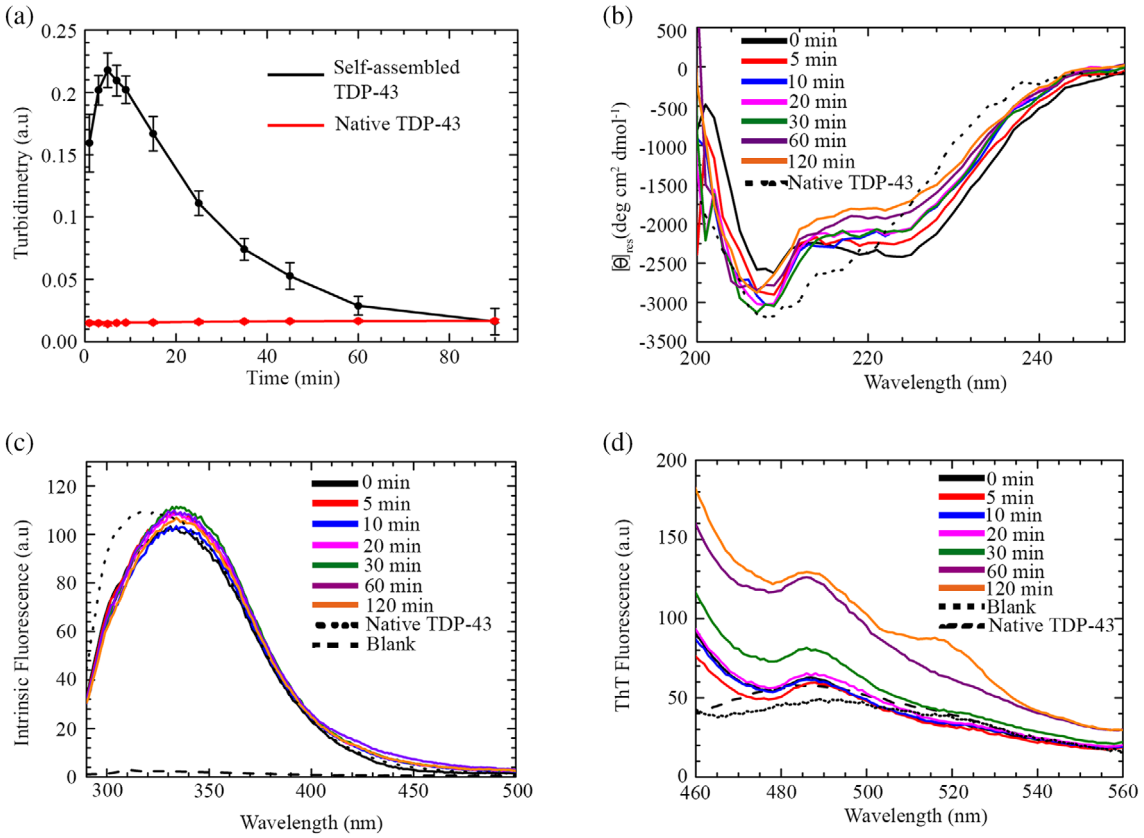

FIGURE 3 Spectroscopic characterization of TDP-43 self-assembly. (a) Time course of TDP-43 self-assembly monitored with turbidimetry. Self-assembly was induced by a solution-jump method, as described in the legend of Figure 2. The time course for native TDP-43 was measured in QFF Buffer B at the same TDP-43 concentration (5 μM). Error bars: *SEM*. (b) Far-UV CD spectra of TDP-43 preincubated at a concentration of 5 μM, in 20 mM acetate, 150 mM NaCl, 5% (wt/vol) PEG 8000, 2 mM TCEP, pH 5 (final pH 6), 25°C, under agitation at 560 rpm from 0 to 120 min. The spectrum of native TDP-43 is in 20 mM Tris–HCl, 150 mM NaCl, pH 8.0 and was previously recorded.[52] (c) Intrinsic fluorescence spectra of TDP-43 preincubated as described above. The spectrum of native TDP-43 is in QFF Buffer B. (d) ThT Fluorescence spectra of TDP-43 preincubated as described above. The spectrum of native TDP-43 is in QFF Buffer B

The first parameter to be varied was pH. Turbidity time courses were recorded at final pH values of 4.0, 5.0, 6.0, and 7.0, while keeping the remaining conditions unchanged (Figure 4a). At all pH values, the time courses featured a rapid increase of OD_{600} at all three salt concentrations, followed by a slower decrease that was evident in all cases, except at the lowest two salt concentrations at pH 4.0. Since the rapid increase is due to formation of individual round assemblies and their small clusters and the slower decrease to their further assembly into larger clusters, these data indicate that these two events occur at all pH values and salt concentrations investigated here, except at pH 4.0 in 0 and 50 mM NaCl, where formation of the first round species was still present but less evident and was not followed by further assembly. Interestingly, the most marked increase of turbidity was found to occur at pH 6.0 and at the highest NaCl concentration: at lower and higher pH values, the initial turbidity increase was less pronounced. This suggests that TDP-43 was strongly phase separated at the pH value that matches the isoelectric point of the protein (theoretical pI = 6.02), and underlines the importance of minimal electrostatic repulsions between protein molecules in self-assembly. A notable exception was found at pH 7, where the highest turbidity was found at 0 and 50 mM NaCl, confirming a change in electrostatic network, residues exposure and interactions.

The second parameter to be varied was protein concentration. We therefore screened different concentrations of TDP-43, again at the three salt concentrations of 0, 50, and 150 mM, while keeping the remaining conditions unchanged (Figure 4b). At 2.5 μM TDP-43, the initial increase of turbidity was very small and delayed and was not followed by a slower decrease or, if any, the decrease was slower than the timescale monitored here, indicating limited phase separation and clustering of the few TDP-43 aggregates. Conversely, at 5, 7.5, and 10 μM TDP-43, the turbidity time courses showed the two typical phases, whose amplitudes and rates were proportional to protein concentration, as expected according to the laws of kinetics.

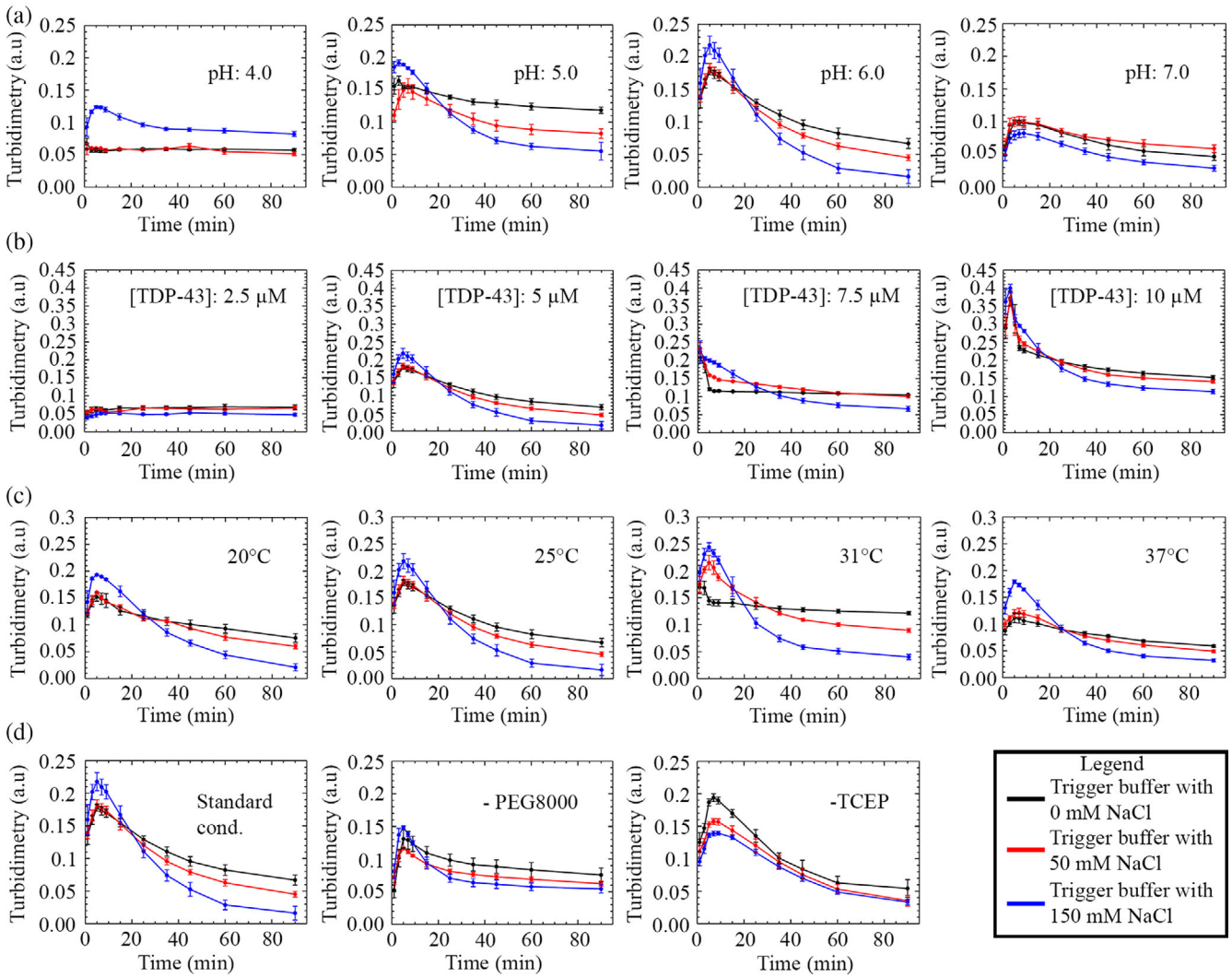

FIGURE 4 Multiparametric dependence of TDP-43 self-assembly monitored by turbidimetry. Final standard conditions were, unless otherwise indicated, 5 μM TDP-43 in 20 mM acetate buffer, pH 5.0 (to reach a final pH 6.0 after dilution), 5% (wt/vol) PEG 8000, 2 mM TCEP, 25°C, containing either 0 mM (black), 50 mM (red), or 150 mM (blue) NaCl, as indicated in the legend box. (a) Turbidity time courses at various final pH values. From left to right: pH 4.0, pH 5.0, pH 6.0, and pH 7.0. (b) Turbidity time courses at various TDP-43 concentrations. From left to right: 2.5 μM, 5 μM, 7.5 M, and 10 μM TDP-43. (c) Turbidity time courses at various temperature values. From left to right: 20, 25, 31, and 37°C. (d) Turbidity time courses in the presence or absence of crowding and reducing agents. From left to right: standard conditions, absence of PEG 8000, absence of TCEP. Error bars: *SEM*

We then carried out a screening under our standard conditions but at various temperature values (Figure 4c). The turbidity kinetics were similar at the four studied temperature values, but the highest OD_{600} value after the first phase was found to occur at 31°C, as if there was an inversion temperature point around 31°C. Higher temperature (37 and 43°C) showed weak phase separation, particularly at 43°C, where turbidity values were the lowest. We did not show our kinetic profiles at 43°C because of strong turbidity due to condensation on the top of the plate lid that affected heavily the measurements after 30 min. Aggregate clustering followed a similar temperature dependence (Figure 4c). In spite of the maximum for aggregate formation and clustering observed at 31°C and decrease in intensity of both phenomena beyond this temperature value, the temperature increase beyond this value led to slightly faster processes in both cases.

Finally, we investigated the effect of PEG 8000 as a crowding agent and TCEP as a reducing agent. The absence of PEG 8000 led to a weaker phase separation compared to that achieved in its presence, as indicated by the lower amplitude of the first phase (Figure 4d). Moreover, the further assembly of the aggregated species occurred to produce smaller species, as judged by the lower amplitude of the second slower phase. The absence of TCEP also led to a weaker phase separation, although

to a much lower extent relative to that observed in the absence of PEG 8000 (Figure 4d).

3 | DISCUSSION

3.1 | Phase separation of TDP-43 is not genuine LLPS

As described in the Sections 1 and 2, with the term "phase separation," we intend a process in which the protein passes from solution into self-assemblies, regardless of their solid or liquid state. We showed that full-length TDP-43 undergoes rapidly (<1 min) phase separation when diluted from its initial solution, in which it was soluble, native, and dimeric, into other solutions in which it was not soluble, specifically at protein concentrations of 2.5–10 μM, pH 4–7, in 0–150 mM NaCl, with or without 5% (wt/vol) PEG 8000 or TCEP, 20–43°C. Using confocal microscopy in fluorescence and bright-field modes, and using a protein labeled with either TMR or Alexa488, we found that the assemblies were apparently round in shape and had a diameter of about 0.5–1.0 μm (although larger species were occasionally seen and smaller species may also have been present and escaped experimental detection). The assemblies, however, were not liquid and the observed phase separation did not consist, therefore, in typical *bona fide* LLPS, which has been observed repeatedly, by contrast, for the TDP-43 CTD.[16,17,47,57] In fact, to be classified as liquid, the assemblies need to satisfy three main hallmarks: (a) roughly spherical shape, (b) ability to coalesce, and (c) rapid molecular rearrangement.[58] The condensates clearly did not coalesce, as they tended to cluster into bunches with irregular shape in which the initial individual condensates were still visible. The first criterium was not, therefore, satisfied. Moreover, the FRAP was partial (∼20%) in all assemblies tested, indicating a gel-like phase rather than a purely liquid phase, leaving also the second hallmark not satisfied. In previous works, although the assemblies were apparently spherical, TEM and super-resolution STED microscopy have shown an irregular structure within them,[36,59] therefore questioning the satisfaction of even the first criterium. Here, we also found that the initial individual round condensates did not have an entirely round or ovoid shape, as they showed an irregular boundary, ruling out the presence of liquid droplets and confirming that our system did not satisfy the first criterium.

These results are in agreement with a previous report in which TDP-43 fused to His tag and YFP (His-YFP-TDP-43) was shown, with confocal fluorescence microscopy, to form speckles that assembled further, without fusing, into irregular flocculent tufts featuring partial FRAP.[36] They are also in agreement with another report in which partial cleavage of TDP-43 fused to the MBP and His tag (TDP-43-MBP-His) to release TDP-43 led to the formation of condensates assembling in a chain-like arrangement and then further clustering, without fusion and with only partial FRAP.[50] Moreover, they are also consistent with other reports showing an inability of the assemblies of TDP-43 linked to other proteins to fuse, as they rather accumulated in strings or form irregularly shaped aggregates, respectively.[24,49] They are not, however, in agreement with results of another report on His-SUMO-TDP-43 and TDP-43-MBP-His in which the droplets appeared spherical and able to fuse.[48]

Unlike our work, all these studies have been carried out with TDP-43 fused to large solubilizing proteins, including SUMO, MBP, YFP, or after proteolysis-mediated TDP-43 release without further purification. Our results indicate that this behavior is retained with TDP-43 in absence of these large tags. One important advantage of our method is the induction of phase separation with a solution-jump method, under conditions in which the protein maintains initially its native state, without influencing the structural conformation of the protein with slow and incomplete cleavage of soluble tags and without producing released tags and leaving unproteolysed protein molecules and the protease itself that may well alter the phase transition process of TDP-43.[60]

3.2 | The multiparametric analysis helps rationalize the driving forces of TDP-43 phase separation and aggregate clustering

To better visualize how the different parameters studied here could affect both phase separation into the first round assemblies and their further clustering, we built up a scheme to indicate the conditions in which the two processes were promoted or inhibited (Figure 5a). For comparison, we also showed in the same scheme the conditions previously found to promote phase separation into liquid droplets of the isolated TDP-43 CTD (Figure 5b). TDP-43 phase separation was found to be promoted as the pH approached a value of 6.0 from either side, by an increase of salt concentration, by an increase of protein concentration, by an increase of temperature up to a value of 31°C, by crowding agents and, to a very small extent, by reducing agents. Further clustering was found to be promoted by exactly the same conditions, indicating that both phase separation and aggregate clustering were essentially governed by similar driving forces.

By contrast, the previously studied phase separation of TDP-43 CTD into liquid droplets was found to have a multiparametric dependence significantly different.

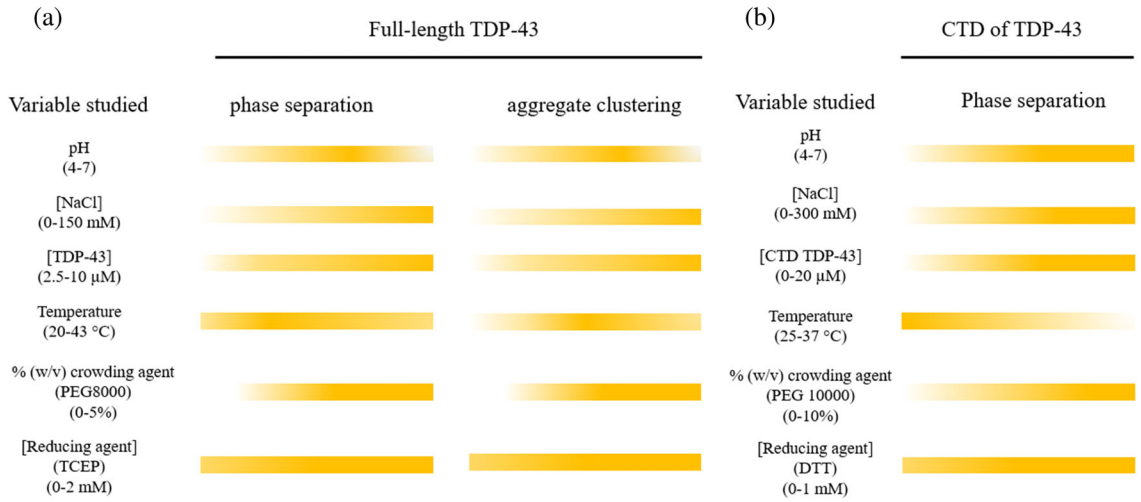

FIGURE 5 Recap scheme indicating the results of the multiparametric screening. Orange and white areas indicate conditions in which phase separation was promoted or inhibited, respectively, for full-length TDP-43 (a) and TDP-43 CTD (b). (a) Variables studied in this work that influence TDP-43 phase separation and aggregate clustering. From top to bottom: pH, [NaCl], [TDP-43], temperature, [PEG 8000], [TCEP]. (b). Variables studied in previous work[47] that influence TDP-43 CTD phase separation. From top to bottom: pH, [NaCl], [TDP-43], temperature, [PEG 8000], [TCEP]. In all cases, the left and right margins of a given bar refer to the lowest and highest values of the indicated variable window

While increases of salt concentration, protein concentration and crowding agents were found to promote LLPS of CTD and reducing agents had very little effect,[17,47] therefore similarly to the results found here for full-length TDP-43 phase separation into gel-like species, the dependences on pH and temperature were different. Phase separation of full-length TDP-43 increased with pH, up to a value of 6.0 and then decreased, unlike the CTD that phase separated linearly with pH.[47] This difference can be explained by the different isoionic points of the two proteins, which are 6.02 (or 5.85 without His-tag) and 9.98, respectively. Hence, the maximum phase separation is achieved at pH 6.0 for full-length TDP-43, whereas that of the CTD keeps increasing beyond neutral pH. This indicates that phase separation is inhibited by electrostatic repulsions between protein molecules and therefore increases when such repulsions are minimal. The observation that both proteins phase separate more effectively at high salt concentrations lends further support to this electrostatics-affected mechanism.

In addition, LLPS of the CTD decreased with temperature, from 3 to 25°C[17] and then from 25 to 37°C,[47] in sharp contrast with the increase observed here for phase separation into gel-like species of full-length TDP-43 up to 31°C. However, the further increase of the temperature beyond 31°C, to 37°C and then 43°C, led to a decrease of phase separation of the full-length protein, in line with the behavior of the CTD reported previously. This behavior is in agreement with a binodal and spinodal phase diagram where at protein concentrations above saturation (C_{sat}), both low and high temperature values inhibit phase separation, which is maximal at intermediate temperature values.[61–63] It may well be that low temperature values inhibit phase separation for full-length TDP-43, where the presence of stable folded domains provides a bonus of solubility under these conditions.[64]

3.3 | Neutral pH values and salts favor TDP-43 solubility, unlike the isolated CTD

The multiparametric results reported here also provide explanations to some of the initial data obtained on the solubility of full-length TDP-43 that were difficult to explain following the increasing knowledge that was being accumulated on the TDP-43 CTD. In fact, most papers showed solubility of the full-length protein at pH 7.4–8.0, even at high salt concentrations[36,48,50,52–54] and we also selected a buffer at pH 8.0 and containing 1 M NaCl as a solubilizing condition for the present work, albeit in the presence of other solubilizing agents, such as PEG 3350, LDAO, and OG. In sharp contrast, the CTD was found to have a solubility against LLPS that decreased dramatically with pH and salt concentration, and appeared very insoluble at neutral pH in the presence of NaCl.[17,47]

Our multiparametric turbidimetry analysis can reconcile these apparently different behaviors of the CTD and full-length protein, because it shows that full-length TDP-43 phase separation and aggregate clustering

collapses from pH 6.0 to pH 7.0, due to the isoionic point, which is 6.02 only for the full-length protein and is 9.98 for the CTD (see above). Moreover, the salt dependence of the full-length protein is inverted at neutral pH, with phase separation inhibited, rather than promoted, at higher salt concentrations, unlike all other conditions tested here. It is therefore likely that this behavior is exacerbated at pH 7.4–8.0 and that the protein achieves the maximum solubility at mildly alkaline pH values and in the presence of salts, although it often requires additional stabilizing agents or soluble tags and well-defined strategies during protein purification.

4 | CONCLUSIONS

We showed a protein phase separation process of full-length TDP-43, induced by a solution-jump method in the absence of large solubilizing tags or contaminating proteins, which led rapidly to formation of apparently round assemblies having a typical diameter in the range of 0.5–1.0 μm, although larger species were also occasionally visualized. The assemblies, however, failed to comply with the three hallmarks of LLPS, as they had limited internal diffusion, as assessed with FRAP, and were unable to fuse into larger yet similarly round assemblies, as they rather tended to cluster into larger species with irregular morphology where the initial assemblies were still observable. Super-resolution STED microscopy also showed the absence of a perfect round morphology with stretched and squashed regions along the borders. This represents an important difference with the previously characterized CTD where a *bona fide* LLPS behavior was observed by many authors working independently of each other. The results of the multiparametric analysis of phase separation, carried out here on full-length TDP-43 and previously on the CTD, have emphasized many similarities, but also important differences, particularly for the pH and temperature dependencies, because the highest tendency of phase separation for TDP-43 was found when the two parameters approached values of 6.0 and 31°C from both sides, following a binodal and spinodal bell-shaped curve phase diagram, whereas LLPS of the CTD was found to increase proportionally with pH and to decrease proportionally with temperature. These differences can be attributed to different isoionic points of the two protein constructs and by the presence of folded domains in the full-length protein that limits its effective aggregation at low temperature. Finally, our multiparametric results explain why the full-length protein is soluble at neutral pH values and high salt concentrations, although requiring additional solubilizing agents, values that are by contrast prohibitive for the CTD solubility.

5 | MATERIALS AND METHODS

5.1 | TDP-43 expression and purification

Human full-length TDP-43 was recombinantly expressed with a His-tag fused to the N-terminus and having sequence MHHHHHHSSGVDLGTENLYFQS before the first residue of TDP-43 (Met1). This protein (referred to in the manuscript simply as TDP-43) was expressed and purified as previously described.[52] Protein expression occurred overnight at 37°C in *Escherichia coli* BL21 (DE3) cells with an induction by 1 mM isopropyl β-D-1-thiogalatoside (IPTG). Bacteria were harvested at 6,790 g for 30 min at 4°C and resuspended in lysis buffer (50 mM Tris–HCl, 0.5 M NaCl, pH 8.0), followed by sonication at 30 W and 20 kHz (6 cycles of 20 s each). The resulting suspension was centrifuged at 20,300*g* for 30 min at 4°C and the pellet containing the IBs was saved and subjected to three consecutive washes using 50 mM Tris–HCl, pH 8.0, 1% (vol/vol) Triton X-100 (wash 1), 50 mM Tris–HCl, pH 8.0, 2 M NaCl (wash 2), and 50 mM Tris–HCl, pH 8.0 (wash 3), with centrifugations at 20,300*g* for 30 min at 4°C between washing steps. The resulting pellet with cleaned IBs was left in 8 M urea overnight, at room temperature under stirring, in order to foster the solubilization of the IBs and denaturation of TDP-43. The day after, the solution was centrifuged at 20,300*g* for 30 min at 4°C and the supernatant was saved and loaded onto 10 ml of HisPur Ni-nitrilotriacetic acid (Ni-NTA) resin (Thermo Fisher Scientific) in a gravity flow column, pre-equilibrated with buffer A (50 mM Tris–HCl, pH 8.0, 0.5 M NaCl, 8 M urea, 10 mM imidazole). The resin was then washed with buffer B (the same as buffer A but containing 25 mM imidazole) and the elution was carried out with buffer C (the same as buffer A but containing 300 mM imidazole). The eluted protein solution (typically 20 ml) was slowly dropped down at 4°C into refolding buffer (typically 400 ml) containing 50 mM HEPES, pH 8.0, 9.6 mM NaCl, 10 mM KCl, 2 mM $CaCl_2$, 2 mM $MgCl_2$, 0.8 M sucrose, 0.5 M L-arginine, 0.6 M guanidine, 0.5% (vol/vol) Triton X-100, 0.2% (wt/vol) (PEG 3350), 1 mM reduced glutathione (GSH), 0.1 mM glutathione disulfide (GSSG), and one tablet of EDTA-free Pierce Protease Inhibitor (Thermo Fisher Scientific) and left at 4°C until further use. Then, the solution containing the refolded protein was concentrated at 4°C by pressurized ultrafiltration using an Amicon stirred cell (Millipore Sigma) with a 10 kDa molecular weight cut-off (MWCO) membrane filter down to about 15 ml and subjected to size-exclusion chromatography (SEC), at 4°C, with an Akta Pure 25 L system (GE Healthcare, Wakesha, WI), using a HiLoad 16/600 Superdex 200 pg column, pre-

equilibrated with SEC buffer (50 mM HEPES, pH 8.0, 0.2 M KCl, 0.1 M imidazole, 0.1% (wt/vol) PEG 3350, 0.1 M sucrose, 0.025% (vol/vol) Triton X-100). Elution was carried out in isocratic method at a flow rate of 0.5 ml/min. The last purification step foreseen an ion exchange chromatography, at 4°C, using a HiTrap Q-Sepharose Fast Flow (QFF) 5 ml column pre-equilibrated with Buffer A QFF (50 mM HEPES, pH 8.0, 0.1% (wt/vol) PEG 3350, 2 mM LDAO). The sample collected after SEC was applied directly and the protein was eluted with a gradient step method in Buffer B QFF (50 mM HEPES, pH 8.0, 0.1% (wt/vol) PEG 3350, 2 mM LDAO, 0.25% (wt/vol) OG, 1 M NaCl). The TDP-43 containing fractions were merged, concentrated at 4°C using Amicon Ultra centrifugal filter units with 10 kDa MWCO down to about 1–2 ml. The concentrated sample was checked by SDS-PAGE and, finally, stored at −20°C. Protein concentration was determined by optical absorbance spectroscopy using a molar extinction coefficient at 280 nm (ε_{280}) of 46,410 M^{-1} cm^{-1}. The final purified protein had the sequence stretch MHHHHHHSSGVDLGTENLYFQS before Met1, contained 436 residues and had a molecular weight of 47,292.53 Da.

5.2 | Dynamic light scattering

Size distribution of purified TDP-43 was determined at 25°C with a Malvern Sizer Nano S DLS device (Malvern Panalytical), temperature controlled with an internal Peltier system, using a small volume 3 × 3 quartz cuvette (45 µl) and in backscatter (173°) method. Final conditions of the sample were 50 µM TDP-43 in buffer B QFF, 25°C. Viscosity and refractive index were set on the instruments at 0.8788 cp and 1.331, respectively.

5.3 | Intrinsic fluorescence spectroscopy

Intrinsic tryptophan fluorescence emission was measured using a Cary Eclipse spectrofluorometer (Agilent) equipped with a thermostated cell holder attached to an Agilent PCB 1500 water Peltier system. Spectra were recorded at 25°C from 290 to 500 nm at 280 nm excitation, using 10 × 2 mm quartz cuvette and excitation and emission slits of 5 nm for checking the protein after purification. Instead, for self-assembly experiments, a 3 × 3 small volume quartz cuvette and slits of 5 nm were used. Final conditions of the samples were 50 µM TDP-43 in buffer B QFF, 25°C (purified native protein) and 5 µM TDP-43 in 20 mM acetate buffer, pH 5.0, 5% (wt/vol) PEG 8000, 2 mM TCEP, 25°C (to reach a final pH 6.0 after dilution), containing either 0 mM or 150 mM NaCl, 25°C (self-assembled protein).

5.4 | Induction of TDP-43 self-assembly

A TDP-43 sample was thawed and spun down at 18,000 g for 15 min at 4°C to remove aggregated protein. Then, the supernatant was concentrated with Amicon Ultra 500 µl centrifugal filter units with 10 kDa MWCO and subjected to desalting through a Sephadex G15 resin column (Pharmacia Fine Chemicals). Protein concentration was determined with NanoDrop One (Thermo Fisher Scientific) and adjusted to 35 µM by dilution. TDP-43 self-assembly was induced by diluting the protein down to 5 µM into aggregation trigger buffers (see table below), following a previously proposed pH jump method[60] and incubating the resulting TDP-43 samples under shaking at 560 rpm on a TS-100 Thermo Shaker (Kisker) at 25°C for 2 hr.

To investigate the conditions in which TDP-43 self-assembles, we carried out a multiparametric and multidimensional analysis, where 18 trigger buffers were designed (see below). We chose 20 mM acetate buffer, pH 5.0, 0 mM, 50 mM, and 150 mM NaCl, 5% (wt/vol) PEG 8000, 2 mM TCEP, 25°C (to reach a final pH 6.0 after dilution), as our three standard conditions and changed the other parameters one by one, including pH, TDP-43 concentration, temperature, presence/absence of PEG 8000 and presence/absence of TCEP. TDP-43 self-assembly was monitored with turbidimetry in all cases and also with confocal microscopy and bright-field microscopy in our three standard conditions.

The trigger buffers used here are:

1. 20 mM acetate buffer, pH 3.0, 0 mM NaCl, 5% (wt/vol) PEG 8000, 2 mM TCEP
2. 20 mM acetate buffer, pH 3.0, 50 mM NaCl, 5% (wt/vol) PEG 8000, 2 mM TCEP
3. 20 mM acetate buffer, pH 3.0, 150 mM NaCl, 5% (wt/vol) PEG 8000, 2 mM TCEP
4. 20 mM acetate buffer, pH 4.2, 0 mM NaCl, 5% (wt/vol) PEG 8000, 2 mM TCEP
5. 20 mM acetate buffer, pH 4.2, 50 mM NaCl, 5% (wt/vol) PEG 8000, 2 mM TCEP
6. 20 mM acetate buffer, pH 4.2, 150 mM NaCl, 5% (wt/vol) PEG 8000, 2 mM TCEP
7. 20 mM acetate buffer, pH 5.0, 0 mM NaCl, 5% (wt/vol) PEG 8000, 2 mM TCEP
8. 20 mM acetate buffer, pH 5.0, 50 mM NaCl, 5% (wt/vol) PEG 8000, 2 mM TCEP
9. 20 mM acetate buffer, pH 5.0, 150 mM NaCl, 5% (wt/vol) PEG 8000, 2 mM TCEP

10. 20 mM mes buffer, pH 6.3, 0 mM NaCl, 5% (wt/vol) PEG 8000, 2 mM TCEP
11. 20 mM mes buffer, pH 6.3, 50 mM NaCl, 5% (wt/vol) PEG 8000, 2 mM TCEP
12. 20 mM mes buffer, pH 6.3, 150 mM NaCl, 5% (wt/vol) PEG 8000, 2 mM TCEP
13. 20 mM acetate buffer, pH 5.0, 0 mM NaCl, 5% (wt/vol) PEG 8000
14. 20 mM acetate buffer, pH 5.0, 50 mM NaCl, 5% (wt/vol) PEG 8000
15. 20 mM acetate buffer, pH 5.0, 150 mM NaCl, 5% (wt/vol) PEG 8000
16. 20 mM acetate buffer, pH 5.0, 0 mM NaCl, 2 mM TCEP
17. 20 mM acetate buffer, pH 5.0, 50 mM NaCl, 2 mM TCEP
18. 20 mM acetate buffer, pH 5.0, 150 mM NaCl, 2 mM TCEP

5.5 | Confocal and bright-field microscopy

Native TDP-43 (45 μM) was labeled with TMR (Invitrogen) in a 1:10 ratio (dye:protein) in buffer B QFF. Self-assembly was induced in standard conditions, as described above. Then, 5 μl of protein sample were spotted at different time points (0, 5, 10, 60 min) onto a clean microscope slide, covered with a 12 mm glass coverslip and then visualized using a TCS SP8 scanning confocal microscopy system (Leica Microsystems) equipped with an argon laser source at 514 nm, under bright-field and fluorescent modes. TMR was excited at 541 nm and fluorescence emission was collected at 550–700 nm.

5.6 | STED microscopy

Native TDP-43 (45 μM) was labeled with TMR (Invitrogen) in a 1:10 ratio (dye: protein) in buffer B QFF, as described above. Self-assembly was induced in standard conditions without any incubation time, and 40 μl of the protein sample were spotted into a well of a μ-Slide 18 well Glass Bottom sterilized plate (Ibidi GmbH). STED xyz images (i.e., z-stacks acquired along three directions: x, y, and z axes) of individual condensates were acquired in bidirectional mode by using a SP8 STED 3X confocal microscope (Leica Microsystems) equipped with the Leica HC PL APO CS2 ×100/1.40 oil White objective and the HyD (hybrid detector). TMR was excited with a 550 nm tuned white light laser and emission collected at 564–599 nm. A series of optical sections (z-stacks) was taken through the condensate depth; images were then deconvolved using the Huygens Professional software version 18.04 (Scientific Volume Imaging B.V.), and the maximum intensity projection of confocal z-stacks was obtained by superimposition. 3D reconstructions and depth coding profiles of deconvolved images were generated from the z-stacks using the Leica Application Suite X (LAS X) software equipped with the 3D Projection Tool (Leica Microsystems).

5.7 | FRAP measurements

Native TDP-43 (45 μM) was labeled with Alexa Fluor 488 (AAT Bioquest) in a 1:10 ratio (dye:protein) in buffer B QFF. Self-assembly was induced in standard conditions without any incubation time, and 40 μl of the protein sample were spotted into a well of a μ-Slide 18 well Glass Bottom sterilized plate (Ibidi GmbH). The FRAP experiment was performed using the LAS AF FRAP Application Wizard on a Leica TCS SP8 ×3 microscope equipped with a Leica HC PL APO CS2 ×100/1.40 oil White objective and the 488-nm laser, at a scan speed of 700 Hz. Two pre-bleaching images were acquired, and photobleaching was then performed in regions of interest (ROIs) at 100% laser intensity for 15,58 s (twenty iterations). Fluorescence recovery was recorded every 5 s up to 145 s. Fluorescence recovery values were normalized to pre-bleaching fluorescence ones (taken as 100%).

5.8 | Turbidimetry

Turbidimetry was assessed using a Synergy H1 Microplate Reader (BioTek), in no binding, chimney well, flat clear bottom 96-well microplate (Greiner, Bio-One) with lid. TDP-43 self-assembly was induced diluting directly the protein sample into every single trigger buffer and then, shaking in continuous way at 567 counts per min for 2 hr at 25°C. Turbidity was detected every 13 s at 600 nm (OD_{600}) in kinetic mode. Turbidimetry measurements were performed in triplicates for each sample and condition, blank subtracted and then averaged. Plots of turbidity versus time were obtained by considering a window of 120 s for the first five points, a window of 600 s for the following four points and 1,800 s for the last two points, averaging all values recorded within that window and reporting a mean value centered in the same window.

5.9 | Far-UV CD

TDP-43 self-assembly was induced in standard conditions as described above. Far-UV CD spectra were collected

over the 200–260 nm wavelength range at 25°C using a Jasco J-810 Spectropolarimeter equipped with a thermostated cell holder attached to an Julabo 200F water bath and a 1 mm pathlength quartz cuvette. Spectra were averaged from eight scans, blank-subtracted and normalized to mean residue ellipticity.

5.10 | ThT fluorescence

TDP-43 self-assembly was induced in standard conditions as described above, with the addition of 25 μM ThT. The resulting fluorescence was recorded at 25°C from 450 to 600 nm, with excitation at 440 nm, an excitation slit of 5 nm and an emission slit of 10 nm, and using the Cary Eclipse spectrofluorometer (Agilent) mentioned above. A small volume 3 × 3 mm quartz cell was used.

5.11 | Statistical analysis

Data were expressed as means ± *SEM*.

AUTHOR CONTRIBUTIONS

Tommaso Staderini: Methodology, investigation (protein purification, protein self-assembly preparations, DLS, CD, ThT assay, Intrinsic fluorescence assay, turbidimetry, confocal microscopy), writing - original draft, writing - review & editing, visualisation (all figures). **Alessandra Bigi:** Investigation (Confocal fluorescence and brightfield microscopy, STED microscopy, FRAP), writing - original draft. **Daniele Mongiello:** Investigation (protein purification, protein self-assembly preparations, DLS, CD, intrinsic fluorescence assay, turbidimetry). **Cristina Cecchi:** Formal analysis, funding acquisition. **Fabrizio Chiti:** Conceptualization, formal analysis, writing – original draft, writing – review & editing, supervision, project administration, funding acquisition.

ACKNOWLEDGMENTS

This work was supported by a full grant from the *Fondazione Italiana di Ricerca per la Sclerosi Laterale Amiotrofica* (AriSLA, project TDP-43-STRUCT), by two grants from Università di Firenze - Fondazione Cassa di Risparmio di Firenze (Projects TDP43SLA and TROTHERALS), by a grant from the Ministero dell'Università e della Ricerca (PRIN Project 2020PBS5MJ), and by the Università degli Studi di Firenze (Fondi di Ateneo).

CONFLICT OF INTEREST

The authors declare no conflicts of interest.

ORCID

Tommaso Staderini https://orcid.org/0000-0001-6993-4408
Alessandra Bigi https://orcid.org/0000-0002-1067-6288
Cristina Cecchi https://orcid.org/0000-0001-8387-7737
Fabrizio Chiti https://orcid.org/0000-0002-1330-1289

REFERENCES

1. Arai T, Hasegawa M, Akiyama H, et al. TDP-43 is a component of ubiquitin-positive tau-negative inclusions in frontotemporal lobar degeneration and amyotrophic lateral sclerosis. Biochem Biophys Res Commun. 2006;351:602–611.
2. Neumann M, Sampathu DM, Kwong LK, et al. Ubiquitinated TDP-43 in frontotemporal lobar degeneration and amyotrophic lateral sclerosis. Science. 2006;314:130–133.
3. Mackenzie IR, Neumannn M, Bigio EH, et al. Nomenclature forneuropathologic subtypesof frontotemporal lobar degeneration: Consensus recommendations. Acta Neuropathol. 2009;117:15–18.
4. Robberecht W, Philips T. The changing scene of amyotrophic lateral sclerosis. Nat Rev Neurosci. 2013;14:248–264.
5. Polymenidou M, Cleveland DW. The seeds of neurodegeneration: Prion-like spreading in ALS. Cell. 2011;147:498–508.
6. Ravits JM, La Spada AR. ALS motor phenotype heterogeneity, focality, and spread: Deconstructing motor neuron degeneration. Neurology. 2009;73:805–811.
7. Cohen TJ, Lee VMY, Trojanowski JQ. TDP-43 functions and pathogenic mechanisms implicated in TDP-43 proteinopathies. Trends Mol Med. 2011;17:659–667.
8. Lukavsky PJ, Daujotyte D, Tollervey JR, et al. Molecular basis of UG-rich RNA recognition by the human splicing factor TDP-43. Nat Struct Mol Biol. 2013;20:1443–1449.
9. Halliday G, Bigio EH, Cairns NJ, Neumann M, Mackenzie IR, Mann DM. Mechanisms of disease in frontotemporal lobar degeneration: Gain of function versus loss of function effects. Acta Neuropathol. 2012;124:373–382.
10. Cascella R, Capitini C, Fani G, Dobson CM, Cecchi C, Chiti F. Quantification of the relative contributions of loss-of-function and gain-of-function mechanisms in TAR DNA-binding protein 43 (TDP-43) proteinopathies. J Biol Chem. 2016;291:19437–19448.
11. Amador-Ortiz C, Lin WL, Ahmed Z, et al. TDP-43 immunoreactivity in hippocampal sclerosis and Alzheimer's disease. Ann Neurol. 2007;61:435–445.
12. Nakashima-Yasuda H, Uryu K, Robinson J, et al. Co-morbidity of TDP-43 proteinopathy in Lewy body related diseases. Acta Neuropathol. 2007;114:221–229.
13. Schwab C, Arai T, Hasegawa M, Yu S, McGeer PL. Colocalization of transactivation-responsive DNA-binding protein 43 and huntingtin in inclusions of Huntington disease. J Neuropathol Exp. 2008;67:1159–1165.
14. Baloh RH. TDP-43: The relationship between protein aggregation and neurodegeneration in amyotrophic lateral sclerosis and frontotemporal lobar degeneration. FEBS J. 2011;278:3539–3549.
15. Rao PPN, Shakeri A, Zhao Y, Calon F. Strategies in the design and development of (TAR) DNA-binding protein 43 (TDP-43) binding ligands. Eur J Med Chem. 2021;225:113753.

16. Conicella A, Zerze G, Mittal J, Fawzi N. ALS mutations disrupt phase separation mediated by α-helical structure in the TDP-43 low-complexity C-terminal domain. Structure. 2016;24:1537–1549.
17. Li HR, Chiang WC, Chou PC, Wang WJ, Huang JR. TAR DNA-binding protein 43 (TDP-43) liquid–liquid phase separation is mediated by just a few aromatic residues. J Biol Chem. 2018;293:6090–6098.
18. Ayala YM, Zago P, D'Ambrogio A, et al. Structural determinants of the cellular localization and shuttling of TDP-43. J Cell Sci. 2008;121:3778–3785.
19. Shiina Y, Arima K, Tabunoki H, Satoh J. TDP-43 dimerizes in human cells in culture. Cell Mol Neurobiol. 2010;30:641–652.
20. Chang CK, Wu TH, Wu CY, et al. The N-terminus of TDP-43 promotes its oligomerization and enhances DNA binding affinity. Biochem Biophys Res Commun. 2012;425:219–224.
21. Zhang YJ, Caulfield T, Xu YF, et al. The dual functions of the extreme N-terminus of TDP-43 in regulating its biological activity and inclusion formation. Hum Mol Genet. 2013;22:3112–3122.
22. Wang YT, Kuo PH, Chiang CH, et al. The truncated C-terminal RNA recognition motif of TDP-43 protein plays a key role in forming proteinaceous aggregates. J Biol Chem. 2013;288:9049–9057.
23. Afroz T, Hock EM, Ernst P, et al. Functional and dynamic polymerization of the ALS-linked protein TDP-43 antagonizes its pathologic aggregation. Nat Commun. 2017;8:45.
24. Wang A, Conicella AE, Schmidt HB, et al. A single N-terminal phosphomimic disrupts TDP-43 polymerization, phase separation, and RNA splicing. EMBO J. 2018;37:e97452.
25. Mackenzie IR, Bigio EH, Ince PG, et al. JQ pathological TDP-43 distinguishes sporadic amyotrophic lateral sclerosis from amyotrophic lateral sclerosis with SOD1 mutations. Ann Neurol. 2007;61:427–434.
26. Brettschneider J, Del Tredici K, Toledo JB, et al. Stages of pTDP-43 pathology in amyotrophic lateral sclerosis. Ann Neurol. 2013;74:20–38.
27. Giordana MT, Piccinini M, Grifoni S, et al. TDP-43 redistribution is an early event in sporadic amyotrophic lateral sclerosis. Brain Pathol. 2010;20:351–360.
28. Braak H, Ludolph A, Thal DR, Del Tredici K. Amyotrophic lateral sclerosis: Dash-like accumulation of phosphorylated TDP-43 in somatodendritic and axonal compartments of somatomotor neurons of the lower brainstem and spinal cord. Acta Neuropathol. 2010;120:67–74.
29. Hasegawa M, Arai T, Nonaka T, et al. Phosphorylated TDP-43 in frontotemporal lobar degeneration and amyotrophic lateral sclerosis. Ann Neurol. 2008;64:60–70.
30. Lin WL, Dickson DW. Ultrastructural localization of TDP-43in filamentous neuronal inclusions in various neurodegenera-tive diseases. Acta Neuropathol. 2008;116:205–213.
31. Thorpe JR, Tang H, Atherton J, Cairns NJ. Fine structural analysis of the neuronal inclusions of frontotemporal lobar degeneration with TDP-43 proteinopathy. J Neural Transm. 2008;115:1661–1671.
32. Arseni D, Hasegawa M, Murzin AG, et al. Structure of pathological TDP-43 filaments from ALS with FTLD. Nature. 2022;601:139–143.
33. Kerman A, Liu NH, Croul S, et al. Amyotrophic lateral sclerosis is a non-amyloid disease in which extensive misfolding of SOD1 is unique to the familial form. Acta Neuropathol. 2010;119:335–344.
34. Cairns NJ, Neumann M, Bigio EH, et al. TDP-43 in familial and sporadic frontotemporal lobar degeneration with ubiquitin inclusions. Am J Pathol. 2007;171:227–240.
35. Capitini C, Conti S, Perni M, et al. TDP-43 inclusion bodies formed in bacteria are structurally amorphous, non-amyloid and inherently toxic to neuroblastoma cells. PLoS One. 2014;9:e86720.
36. Sun Y, Medina Cruz A, Hadley KC, et al. Physiologically important electrolytes as regulators of TDP-43 aggregation and droplet-phase behavior. Biochemistry. 2019;58:590–607.
37. Colombrita C, Zennaro E, Fallini C, et al. TDP-43 is recruited to stress granules in conditions of oxidative insult. J Neurochem. 2009;111:1051–1061.
38. Chen Y, Cohen T. Aggregation of the nucleic acid-binding protein TDP-43 occurs via distinct routes that are coordinated with stress granule formation. J Biol Chem. 2019;294:3696–3706.
39. McGurk L, Lee VM, Trojanowksi JQ, Van Deerlin MV, Lee EB, Bonini NM. Poly-A binding protein-1 localization to a subset of TDP-43 inclusions in amyotrophic lateral sclerosis occurs more frequently in patients harboring an expansion in *C9orf72*. J Neuropathol Exp. 2014;73:837–845.
40. Gasset-Rosa F, Lu S, Yu H, et al. Cytoplasmic TDP-43 demixing independent of stress granules drives inhibition of nuclear import, loss of nuclear TDP-43, and cell death. Neuron. 2019;102:339–357.e7.
41. Wang C, Duan Y, Duan G, et al. Stress induces dynamic, cytotoxicity-antagonizing TDP-43 nuclear bodies via paraspeckle LncRNA NEAT1-mediated liquid-liquid phase separation. Mol Cell. 2020;79:443–458.e7.
42. Nishimoto Y, Nakagawa S, Hirose T, et al. The long non-coding RNA nuclear-enriched abundant transcript 1_2 induces paraspeckle formation in the motor neuron during the early phase of amyotrophic lateral sclerosis. Mol Brain. 2013;6:31.
43. Wang IF, Narsa MR, Shen CKJ. Higher order arrangement of the eukaryotic nuclear bodies. Proc Natl Acad Sci U S A. 2002;99:13583–13588.
44. Udan-Johns M, Bengoechea R, Bell S, et al. Prion-like nuclear aggregation of TDP-43 during heat shock is regulated by HSP40/70 chaperones. Hum Mol Genet. 2014;23:157–170.
45. Hans F, Glasebach H, Kahle P. Multiple distinct pathways lead to hyperubiquitylated insoluble TDP-43 protein independent of its translocation into stress granules. J Biol Chem. 2020;295:673–689.
46. Ratti A, Gumina V, Lenzi P, et al. Chronic stress induces formation of stress granules and pathological TDP-43 aggregates in human ALS fibroblasts and iPSC-motoneurons. Neurobiol Dis. 2020;145:105051.
47. Babinchak WM, Haider R, Dumm BK, et al. The role of liquid–liquid phase separation in aggregation of the TDP-43 low-complexity domain. J Biol Chem. 2019;294:6306–6317.
48. McGurk L, Gomes E, Guo L, et al. Poly(ADP-ribose) prevents pathological phase separation of TDP-43 by promoting liquid demixing and stress granule localization. Mol Cell. 2018;71:703–717.e9.

49. Molliex A, Temirov J, Le J, et al. Phase separation by low complexity domains promotes stress granule assembly and drives pathological fibrillization. Cell. 2015;163:123–133.
50. Gruijs da Silva LA, Simonetti F, Hutten S, et al. Disease-linked TDP-43 hyperphosphorylation suppresses TDP-43 condensation and aggregation. EMBO J. 2022;41:e108443.
51. Comert F, Dubin PL. Liquid-liquid and liquid-solid phase separation in protein-polyelectrolyte systems. Adv Colloid Interface Sci. 2017;239:213–217.
52. Vivoli Vega M, Nigro A, Luti S, et al. Isolation and characterization of soluble human full-length TDP-43 associated with neurodegeneration. FASEB J. 2019;33:10780–10793.
53. Fang YS, Tsai KJ, Chang YJ, et al. Full-length TDP-43 forms toxic amyloid oligomers that are present in frontotemporal lobal dementia-TDP patients. Nat Commun. 2014;5:4824.
54. Doke AA, Jha SK. Effect of In vitro solvation conditions on inter- and intramolecular assembly of full-length TDP-43. J Phys Chem B. 2022;126:4799–4813.
55. LeVine H 3rd. Thioflavin T interaction with synthetic Alzheimer's disease beta-amyloid peptides: Detection of amyloid aggregation in solution. Protein Sci. 1993;2:404–410.
56. Xue C, Lin YT, Chang D, Guo Z. Thioflavin T as an amyloid dye: Fibril quantification, optimal concentration and effect on aggregation. R Soc Open Sci. 2017;4:160696.
57. Choi KJ, Tsoi PS, Moosa MM, et al. A chemical chaperone decouples TDP-43 disordered domain phase separation from fibrillation. Biochemistry. 2018;57:6822–6826.
58. Gopal PP, Nirschl JJ, Klinman E, Holzbaur EL. Amyotrophic lateral sclerosis-linked mutations increase the viscosity of liquid-like TDP-43 RNP granules in neurons. Proc Natl Acad Sci U S A. 2017;114:E2466–E2475.
59. Cascella R, Banchelli M, Ghadami SA, et al. An *in situ* and *in vitro* investigation of cytoplasmic TDP-43 inclusions reveals the absence of a clear amyloid signature. Ann Med. 2022; 54. https://doi.org/10.1080/07853890.2022.2148734
60. Van Lindt J, Bratek-Skicki A, Nguyen PN, et al. A generic approach to study the kinetics of liquid–liquid phase separation under near-native conditions. Commun Biol. 2021;4:77.
61. Franzmann TM, Alberti S. Prion-like low-complexity sequences: Key regulators of protein solubility and phase behavior. J Biol Chem. 2018;294:7128–7136.
62. Nott TJ, Petsalaki E, Farber P, et al. Phase transition of a disordered nuage protein generates environmentally responsive membraneless organless. Mol Cell. 2015;57:936–947.
63. Ruff KM, Roberts S, Chilkoti A, Pappu RV. Advances in understanding stimulus-responsive phase behavior of intrinsically disordered protein polymers. J Mol Biol. 2018;230:4619–4635.
64. Rosenberger F, Howard SB, Sowers JW, Nyce TA. Temperature dependence of protein solubility—Determination and application to crystallization in X-ray capillaries. J Cryst Growth. 1993;129:1–12.

SUPPORTING INFORMATION

Additional supporting information can be found online in the Supporting Information section at the end of this article.

How to cite this article: Staderini T, Bigi A, Mongiello D, Cecchi C, Chiti F. Biophysical characterization of full-length TAR DNA-binding protein (TDP-43) phase separation. Protein Science. 2022;31(12):e4509. https://doi.org/10.1002/pro.4509